Seeing measurements with autonomous, short-baseline shadow band rangers

Guus Sliepen[a,b], Aswin P.L. Jägers[a,b], Felix C.M. Bettonvil[a,b] and Robert H. Hammerschlag[a],

[a]Astronomical Institute, Utrecht University, Princetonplein 5, 3584 CC Utrecht, the Netherlands
[b]Technology Foundation STW, Utrecht, the Netherlands

ABSTRACT

There is growing interest in measuring seeing at existing and prospective telescope sites. Several methods exist to quantify seeing, one among them is by measuring the scintillation of solar or lunar light using a photodiode. A shadow band ranger (SHABAR) analyses the covariance of the signals from an array of such photodiodes, which allows for the spatial resolution of the index of refraction above the SHABAR device. This allows one to estimate the index of refraction structure parameter as a function of height, $C_n^2(h)$.

Although a SHABAR has a limited range compared to a differential image motion monitor (DIMM) or the latest wavefront sensors, the advantage is that it does not need telescope optics to work. A SHABAR device can be made very compact and can operate independent of other instruments. We describe the design of such a SHABAR device with six photodiodes that can operate virtually indefinitely without requiring human intervention.

An inversion algorithm is used to convert the raw scintillation signals of the photodiodes to the desired $C_n^2(h)$ profile and a value for the Fried parameter r_0 at height zero. We show that it is possible to perform inversions of 10 s periods in real time on relatively low-end hardware, such as an Intel Atom based computer, which allows the results to be presented live to astronomers, who can use this information to help make decisions about their observation schedule.

Keywords: Scintillation, seeing measurements, shadow-band ranger

1. INTRODUCTION

As part of the design study for the European Solar Telescope (EST), several instruments have been created and installed recently[1] to measure seeing at existing telescopes and at prospective telescope sites. The Instituto de Astrofísica de Canarias (IAC) has constructed two long-baseline SHABARs, to be placed on La Palma and Tenerife. which measure the seeing in the lower levels of the atmosphere. The University of Utrecht (UU) has been complementing this effort by constructing five short-baseline SHABAR units, which will be placed at existing telescopes on both sites. The advantage of placing SHABARs at existing telescopes is that the seeing measured by such a SHABAR can be compared to seeing as measured by the telescope with other techniques, such as by the descpeckling of science images or with a wide-field wavefront sensor.

In the design of the short-baseline SHABAR, we have focused on creating a cost-effective unit that is simple to install, and which does not require a human operator. Furthermore, the design of the scintillometers and data reduction software is such that the results can easily be compared with those of the long-baseline SHABARs, and with the SHABAR units that have been used during site testing campaigns for the Advanced Technology Solar Telescope (ATST).[2]

Two of the short-baseline SHABARs have already been installed permanently at the Dutch Open Telescope[5] (DOT) and Swedish Solar Telescope[6] (SST). A third is scheduled to be installed on the GREGOR telescope[7] on Tenerife. A fourth is currently used for testing purposes, and will likely be placed at another telescope on La Palma in the future. A fifth is a mobile unit which, using solar power, can operate completely autonomously in the field for a number of days.

Send correspondence to G. Sliepen <G.Sliepen@uu.nl>, phone: +31 (0)30 253 1617, web: http://dot.astro.uu.nl/

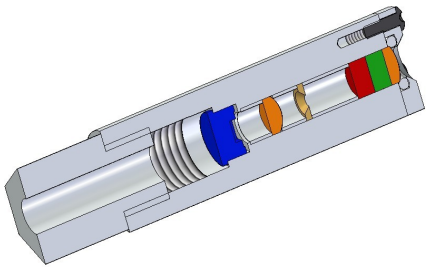

Figure 1. One scintillometer unit. Sunlight enters through a collimator lens (orange) on the top right, through two filters (green and red), a field stop (beige), and an imaging lens (orange), onto the photodiode (blue). A coax cable (not drawn in this picture) exits through a cable gland on the bottom left.

Scintillometer	Position (mm)
1	0.0
2	20.0
3	55.2
4	117.7
5	228.1
6	423.4

Table 1. Positions of the scintillometers relative to the start of the bar.

2. DESIGN

The SHABAR consists of 6 scintillometers that are inserted in holes in a 50 cm long bar. The bar is connected via arm to a motorized iOptron SmartStar mount, which can be controlled via a computer. A camera is mounted on the bar, facing in the same direction as the scintillometers, that is used to track the Sun during the day. The camera housing and scintillometers are weatherproof. A flexible plastic jacket encloses the mount to ensure it is weatherproof as well. The mount is placed on a corner piece on top of a metal pipe, such that it is roughly aligned with the equator. All cable go through the pipe, and then to an enclosure containing the scintillometer amplifier, analog-to-digital converted and computer. The computer can be connected via Ethernet or WiFi to a nearby network. The computer runs a tracking algorithm and logs the raw scintillometer data to disk. Optionally, it can perform a rough inversion of the raw data. A live stream of the captured (and optionally inverted) data can be requested from the computer via the network to allow live view of the data.

2.1 Scintillometer units

Each scintillometer unit consists of a cylindrical, weatherproof housing made of anodized aluminium, containing a Hamamatsu S2386-44K photodiode, two bandpass filters (KG3 and BG13), two lenses and a field stop (see figure 1). The photodiode sits in a socket to which a coaxial cable is connected. The cable exits the unit through a stainless steel cable gland. The unit can be disassembled completely, allowing components to be replaced if necessary. An O-ring at the top and a rubber ring in the cable gland make the unit water resistant. The design is similar to that used for the ATST site testing, so that it will be easy to compare data taken with the new SHABARs with that taken for the ATST.

2.2 Bar

The bar is a hollow, rectangular profile bar of anodized aluminium. There are circular holes drilled in it at intervals corresponding to the desired detector separations (see table 1). Each scintillometer unit fits tightly through a hole, and is fixed with a single screw. The separations are chosen to be equal to the smallest 6 separations of the long-baseline SHABAR, so that it will be easy to compare data from the long- and short-baseline SHABARs.

2.3 Camera unit

The camera unit consists of a custom made weatherproof housing created from white arnite. The circuit board of a Logitech QuickCam 3000, with CCD and lens, are put inside the housing. A circular piece of welding glass covers the circuit board, preventing overexposure of the CCD from the Sun, and at the same time blocking out anything else from the image. The

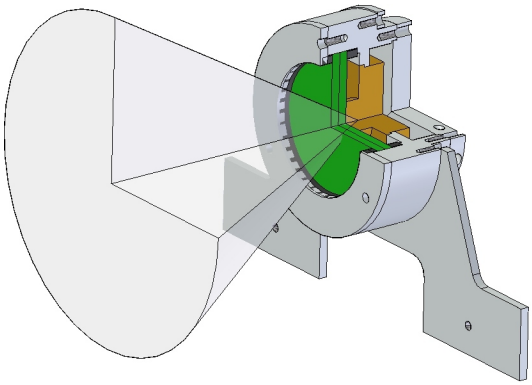

Figure 2. The camera unit, with the QuickCam board (orange) mounted behind welding glass (green). A USB cable (not drawn in this picture) exits through the back of the unit.

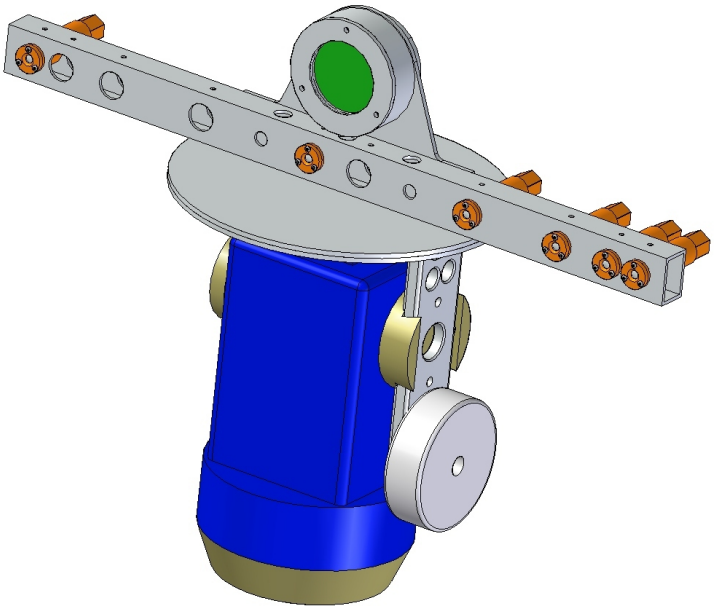

Figure 3. The iOptron mount (blue) with the scintillometer units (orange) and camera unit mounted on it.

welding glass and circuit board are held in place by a neoprene ring (which keeps the unit water resistant) and a cover plate (see figure 2). The USB cable attached to the circuit board exits through a gland at the back of the unit. The whole camera unit is rigidly fixed to the bar with two screws, such that the camera is looking in roughly the same direction as the scintillometer units. With the lens that comes with the camera, the field of view of the camera is 54 degrees. The use of a guider camera avoids the need to have to align the SHABAR unit precisely.

2.4 Mount

In order to keep the scintillometers pointing at the Sun all the time, a iOptron GotoNova mount is used. This is a small, compact mount which can be controlled via a computer. To protect the mount from humidity and rain, it is covered by a flexible plastic sleeve. The sleeves will be replaced by rubber gaiters that will be fixed to the hour axis of the mount (the blue part in figure 3).

2.5 Electronics

The photodiodes are connected to a scintillometer amplifier box designed by the IAC. The photodiodes are driven in photovoltaic mode. The output signal of each photodiode first goes through a pre-amplification stage with configurable

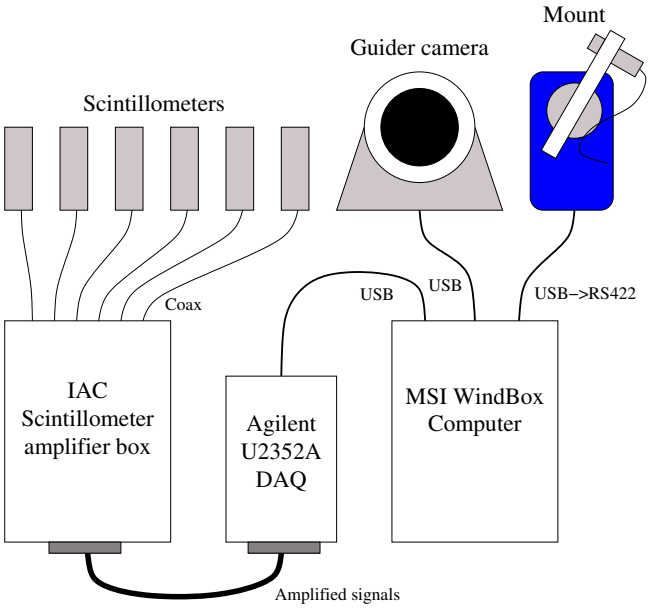

Figure 4. Overview of the electronics used for the SHABAR.

gain. A butterworth filter is then used to split the signal into a high frequency (> 0.1 Hz) AC component and a low frequency (< 0.1 Hz) DC component. The high frequency component is then amplified with a fixed gain of 100. The gain of the pre-amplification stage is set so that when the Sun is in zenith on a clear day, the DC output is approximately -7 V.

All the AC and DC outputs of the amplifier box are connected to the analog inputs an Agilent U2352A USB DAQ box. The grounds of the amplifier box outputs are all connected to the analog reference input of the DAQ. This device has 16 analog inputs, and has a 16 bit ADC that can sample at more than 1 MHz. The maximum range of the input signal is $-10 \ldots 10$ V. All inputs are sampled in short bursts at a rate of 1 kHz, and the data is sent via USB to an attached computer (see figure 4).

The computer is an MSI Wind Box, chosen for its small size and completely fanless operation. It contains an Intel Atom N270 CPU, 1 GB RAM, has a 160 GB harddisk, and has three USB ports, Ethernet and WiFi. A Debian GNU/Linux distribution is installed on it.

2.6 Tracking

In order to keep the SHABAR pointing towards the Sun, regardless of any alignment errors, the relative position of the Sun is continuously tracked using the camera attached to the SHABAR. The processing of the camera images is very simple. First, a threshold is applied that rejects any pixels with a low intensity, to remove readout noise. Then, a simple center of mass algorithm determines the center of the image of the Sun. Although the diameter of the Sun on the CCD is only 6 pixels, the lens has been placed such that the image is slightly out of focus, removing aliasing effects, which results in a very good sub-pixel resolution. The effective resolution of the tracker is approximately 10 arcsec.

The tracking software implements a simple servo loop, which tries to keep the Sun in the center of the camera image as closely as possible. To keep the motion as smooth as possible, only proportional feedback is used with a low gain. To allow for slight differences in the orientation of the camera with respect to the scintillometers, a configurable offset is applied to the calculated center of the image. The offset is chosen such that the DC component of the scintillometers is at its peak.

When the Sun is obscured by clouds, the tracking software will estimate the position of the Sun according to the current time, assuming a roughty equatorial mounting of the SHABAR.

2.7 Data acquisition

The raw data from the DAQ is received by the computer. First, the AC components are divided by their respective DC components, to cancel any differences in the pre-amplifier gain of each scintillometer, and to make the AC signal independent of the mean intensity of the Sun.

Then, the average DC component of each of the 6 scintillometers, and 21 cross-covariance values from the AC signals each of the possible pairs of scintillometers are calculated for 2 and 10 s periods. The resulting values are stored to disk, along with timestamps. Although the 10 s period has been used by the ATST site testing campaign, experience has shown that seeing fluctuates at much smaller timescales, and a shorter period is necessary to better compare the results from the SHABAR to that of the results from the wide-field wavefront sensor at the SST.

2.8 Inversion

To calculate C_n^2 profiles and r_0 values from the covariances, the same procedure as described by F. Hill et al.[3] for the ATST site testing is used. The IDL procedures that were included in that report were rewritten in C, to allow the inversion to run on small computers without the need to install an IDL environment.

It is assumed that seeing effects come from a number of thin, turbulent layers at different heights in the atmosphere. Further, it is assumed that the turbulence in each layer can be described with Kolmogorov statistics. A set of $N_h = 20$ heights from 1 m to 20 km is chosen with equidistant steps on a logarithmic scale:

$$h_i = 20000^{(i-1)/(N_h-1)}, \quad i = 1 \ldots N_h \tag{1}$$

Then, for each time period, the kernels $K_{i,j}$ are computed for each height and each of the N_r possible detector separations r, taking into account the zenith angle ζ from that period:

$$K_{i,j} = 0.38 \frac{32\pi h_i^2 \sec^3 \zeta}{(a + \alpha h_i \sec \zeta)^2} Q\left(\frac{r_j}{a + \alpha h_i \sec \zeta}\right), \tag{2}$$

where $a = 0.002$ m is the diameter of the photodiode, $\alpha = 0.0093$ is the width/height ratio of the cone extending from the scintillometer to the Sun, and

$$Q(s) = \int_0^\infty [J_1(\pi f)]^2 J_0(2\pi f s) f^{-2/3} \mathrm{d}f. \tag{3}$$

Since calculating $Q(s)$ with enough accuracy takes a long time, it has been pre-computed. Unlike the IDL code from RPT-0014, the pre-computation is done with equidistant steps on a logarithmic scale, since the function $Q(s)$ changes rapidly in the beginning, but becomes increasingly smooth as s increases. When calculating the kernels, linear interpolated values from the pre-computed function are used.

The kernels describe how much the structure function at a particular height, $C_n^2(h)$, contributes to the covariance for each possible detector separation measured at the level of the SHABAR. As can be seen in figure 5, the kernels rapidly converge at heights greater than 1 km, which limits the effective range of a SHABAR. Given $C_n^2(h)$ the modeled covariances $B_I(r)$ are given by the following formula:

$$B_I(r) = \sum_{i=1}^{N_h} C_n^2(h_i) \cdot K(h_i, r) \tag{4}$$

The Nelder-Mead algorithm, also known as the amoeba algorithm, is then used to determine which values for $C_n^2(h)$ would best fit the observed covariances, by minimising the mean squared difference between the measured covariances $B_j(r)$ and the modeled covariances $B_I(r)$, given by following function:

$$E_m = \frac{1}{N_r} \sum_{i=1}^{N_r} (B_j(r_i) - B_I(r_i))^2 \tag{5}$$

Since there are more heights than detector separations, a restriction is applied to the possible C_n^2 values: the slope of the C_n^2 curve should be smooth on a logarithmic scale. This is implemented by adding another term to the minimization function used by the amoeba algorithm:

$$E_s = \frac{1}{2(N_h - 1)} \sum_{i=2}^{N_h} \left(\log C_n^2(h_i) - \log C_n^2(h_{i-1})\right)^2 \tag{6}$$

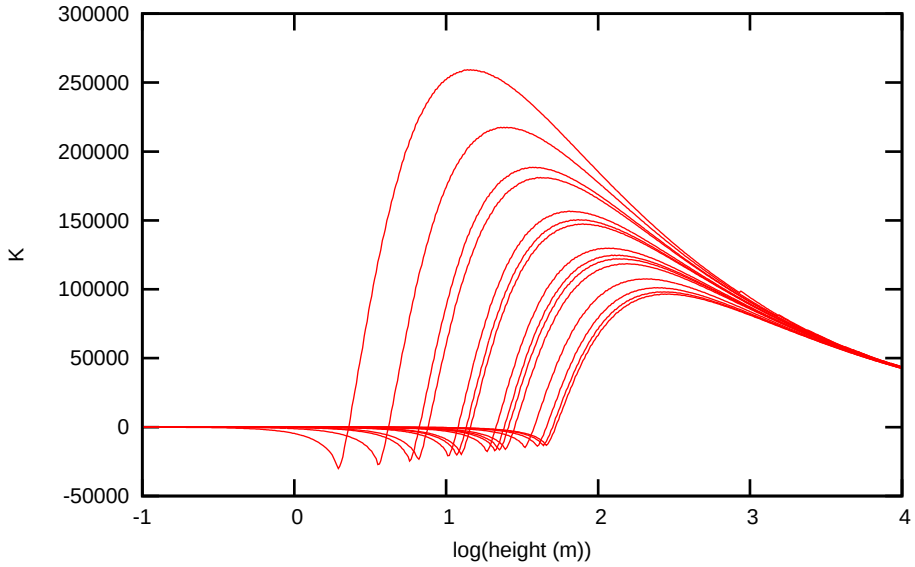

Figure 5. The kernels K_j as a function of height for each of the detector separations of the UU short-baseline SHABARs.

Figure 6. A SHABAR installed on the DOT, without a protective jacket covering the mount.

The strength of the second term is controlled via the parameter λ, resulting in the following complete minimization function:

$$E = E_m + \lambda E_s \tag{7}$$

In order to ensure that the resulting inversions are reasonably smooth, but that it does not constrict the results so much that it doesn't allow situations where most seeing contributions come from a single height, we have set $\lambda = 10^{-15}$.

To allow for a live display of the seeing, the amoeba algorithm can be restricted in the number of steps it performs. When there is reasonably good seeing, the changes in seeing from one period to the next are also smaller. The result of the previous inversion is used as one of the starting point for the next inversion, allowing the amoeba algorithm to approach a solution quicker. However, the size of the initial simplex is reset to that of the expected solution space for each run to avoid having to perform many expanding steps before being able to approach the new minimum, and to avoid the possibility that the simplex from the previous run is completely contained in a local minimum of the next run.

Figure 7. A SHABAR installed on the SST, on a 2 m high metal tube, with a plastic jacket covering the mount. On the fence to the left, an enclosure is mounted containing all the electronics. Only power and Ethernet cable go into the SST building.

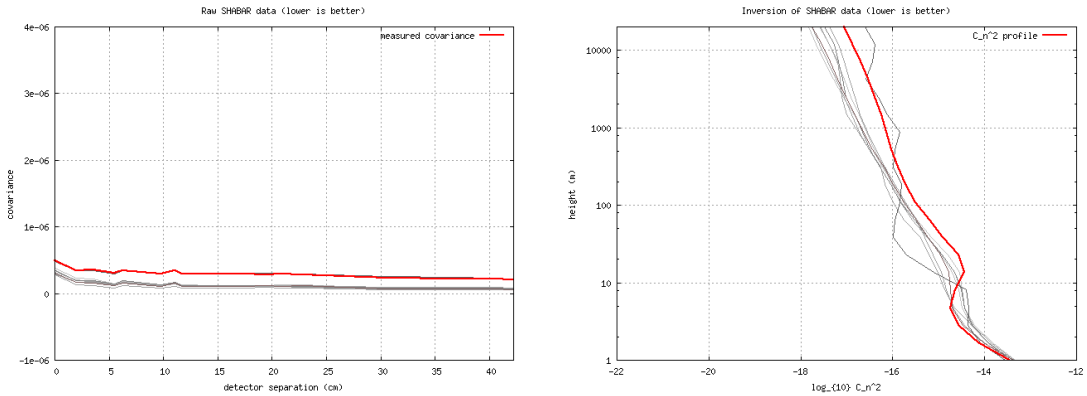

Figure 8. Measured covariances (left) and the resulting inversion (right). The red lines are the values from a certain 10 second period, the grey lines are values from the immediately preceding periods, showing how things vary over time.

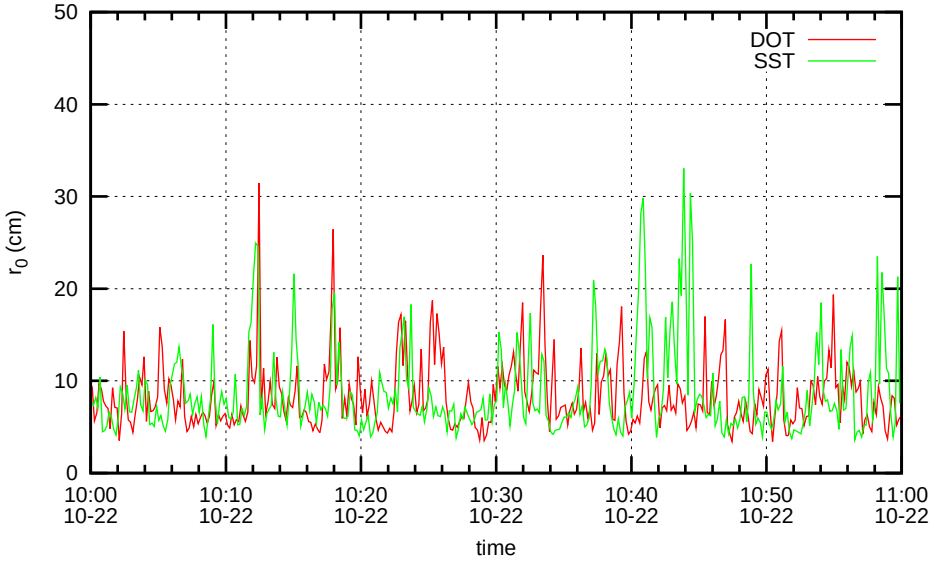

Figure 9. One hour plot of r_0 measured at the DOT and the SST.

3. INSTALLATION ON DOT AND SST

At the moment of writing, two SHABARs are completely finished, and have been installed on top of the DOT and the SST. Since the wind comes mostly from the north, both units have been placed a few meters north of each telescope, so that there is a smaller chance that the low level seeing, as seen by the SHABAR, is disturbed by the telescope structure. Both units are in operation, and data is being captured and inverted in real time.

4. FUTURE INSTALLATIONS

A third SHABAR will be installed on the GREGOR telescope in the summer of 2010. A fourth SHABAR will probably be installed on one of the telescopes on La Palma by the end of 2010. A fifth, mobile SHABAR is equiped with a large battery and two solar panels, allowing it to work completely autonomously for several days in the field. A portable mast will be constructed to allow the mobile SHABAR to be set up in the field above the ground level seeing.

5. FIRST RESULTS

The SHABARs on the DOT and SST have been running since October 15, 2009. However, due to the sensitivity to ice, the SHABARs have been removed for the duration the winter period. An example of the measured covariance as function

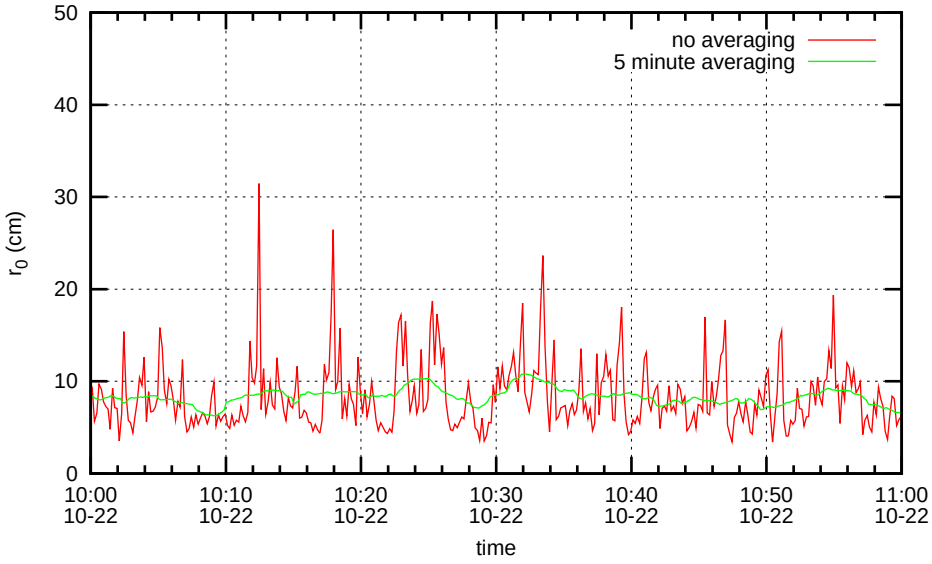

Figure 10. One hour plot of r_0 measured at the DOT, with and without the application of a 5 minute sliding average.

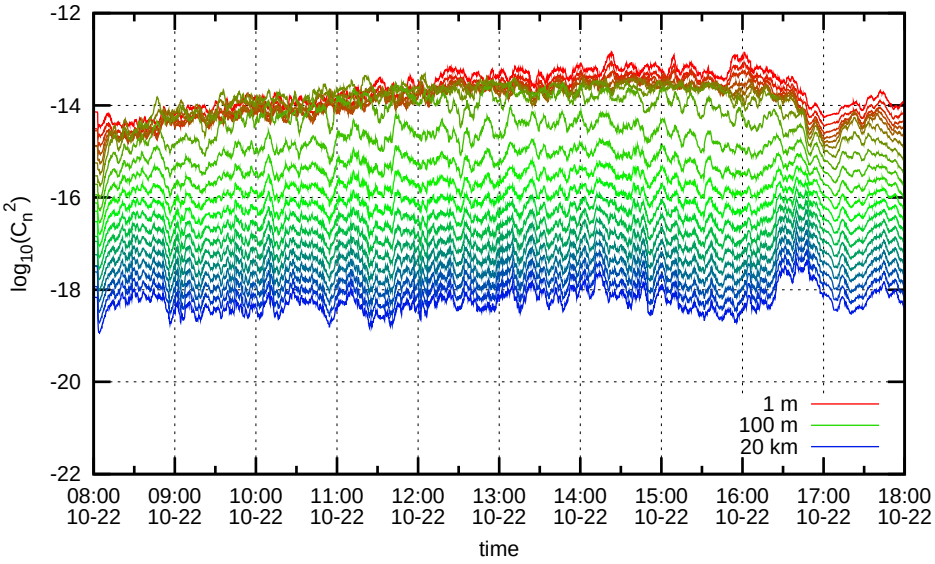

Figure 11. One day of $C_n^2(h)$ measured at the DOT. Each line corresponds to a specific height.

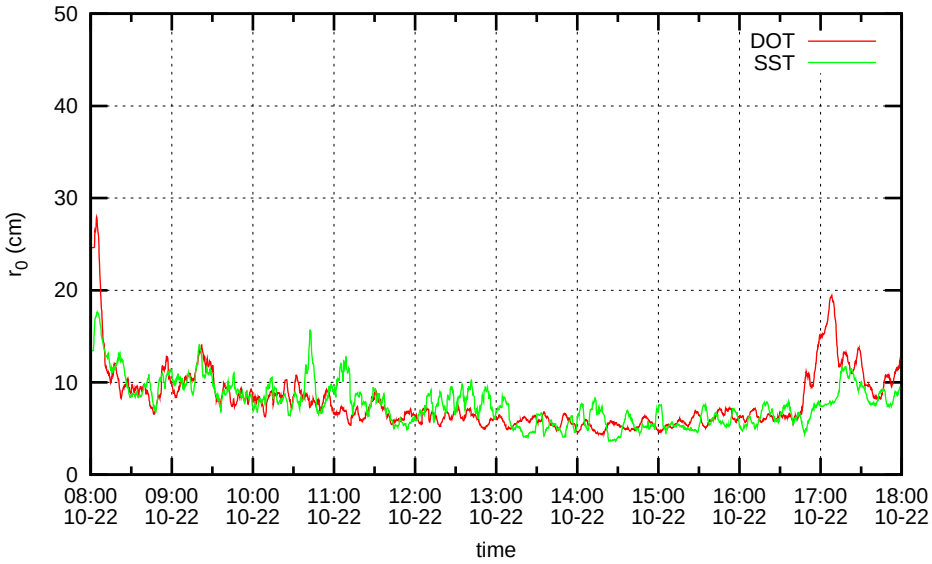

Figure 12. One day of r_0 measured at the DOT and the SST, showing the trend typical for La Palma.

of detector separation, and the corresponding inversion, has been plotted in 8. A plot of r_0 from one hour of October 22 has been plotted in 9. As can be seen, there are large variations in the measured seeing over time. Many peaks of r_0 from both the DOT and SST coincide, suggesting that these large variations are not caused by noise. However, the peak values for r_0 are very large, which raised some questions. The r_0 values calculated as a result from the DOT despeckle process for instance, have never been larger than 16 cm. The DOT typically takes bursts of 100 images at 10 Hz, corresponding to a 10 s period, the same as is used for the inversion of the SHABAR data. However, a likely explaination is that there is a large contribution to telescope seeing from higher layers in the atmosphere that the SHABAR is insensitive to. Comparison with results from the wide-field wavefront sensor (WFWFS) at the SST will be done to further investigate this effect, since the WFWFS measures differential image motion of 85 subapertures with a field-of-view of only 5.5×5.5 arcsec, allowing it to probe $C_n^2(h)$ accurately to much greater heights than a SHABAR.[4]

A 5 minute sliding average will be applied to the data to get a smoother and more realistic value for r_0, as can be seen in figure 10. The averaged results for a whole day are plotted in figure 12. As can be seen, $r_0 \approx 10$ cm at the start of the day, decreasing to 5 cm around noon, as is typical for La Palma. At the end of the day, r_0 increases again. Both SHABARs show the same daily trend, but there are of course variations between the two telescopes.

6. ACKNOWLEDGEMENTS

The Technology Foundation STW in the Netherlands supports this work financially under grant 06640, in collaboration with the Institute for Solar Physics of the Royal Swedish Academy of Sciences. This work is also carried out as a part of the Collaborative Project ”EST: The large-aperture European Solar Telescope”, Design Study, funded by the European Commissions 7th Framework Programme under grant agreement no. 212482.

Technical support comes from the SST, GREGOR and DOT groups. The SST is operated by the Institute for Solar Physics of the Royal Swedish Academy of Sciences, associated with the Stockholm University. The GREGOR is operated by the German consortium of the Kiepenheuer Institut für Sonnenphysik, the Astrophysikalisches Institut Potsdam, the Institut für Astrophysik Göttingen and other national and international partners at the Observatorio del Teide (OT) on Tenerife. The DOT is operated by Utrecht University at the Observatorio del Roque de los Muchachos (ORM) on La Palma. All three observatories are operated by the Instituto de Astrofsica de Canarias in Spain. The DOT has been built by instrumentation groups of Utrecht University, the Central Workshop of Delft University (now DEMO-TU-Delft) and several firms with specialized tasks with funding from the Technology Foundation STW. The DOT team enjoys hospitality at the solar telescope building at ORM of the Royal Swedish Academy of Sciences.

REFERENCES

1. Th. Berkefeld, F. Bettonvil, M. Collados, R. López, Y. Martín, J. Peñatec, A. Pérez, G. Scharmer, G. Sliepen, D. Soltaua, T. Waldmanna and T. van Werkhoven, "Site-seeing measurements for the European Solar Telescope", Astronomical Instrumentation, Proc. SPIE **7733-164**, 2010.
2. F. Hill et al., "Site testing for the Advanced Technology Solar Telescope", Astronomical Instrumentation, Proc. SPIE **6267**, 2006.
3. F. Hill, R. Radick and M. Collados, "Deriving $C_n^2(h)$ from a Scintillometer Array", ATST Site Survey Working Group Final Report. ATST Proj. Doc., 14, `http://atst.nso.edu/files/docs/RPT-0014.pdf`
4. G. B. Scharmer and T. van Werkhoven, "S-DIMM+ height characterization of day-time seeing using solar granulation", Astronomy and Astrophysics, **513**, 2010.
5. Dutch Open Telescope, `http://dot.astro.uu.nl/`.
6. Swedish Solar Telescope, `http://www.solarphysics.kva.se/`.
7. GREGOR telescope, `http://gregor.kis.uni-freiburg.de/`.